Study of a twisted ATLAS SCT Barrel deformation as revealed by a photogrammetric survey

E. Dobson, S.M. Gibson, F. Heinemann, M. Karagöz Ünel
University of Oxford, DWB, Keble Road, OX1 3RH, UK

July 28, 2008

1 Abstract

A photogrammetry survey on the SCT barrels was performed as an engineering check on the structure of the ATLAS Semiconductor Tracker (SCT) shortly after construction. Analysis of the data obtained revealed small scale elliptical deformation as well as a twist of the structure. The results of the survey are presented as well as interpolation of the measured targets to the module positions and a comparison with track based alignment measurements from cosmic ray data.

Contents

2 Introduction

2.1 Overview of the ATLAS Inner Detector and the Semiconductor Tracker

The closest section of the ATLAS detector to the interaction point is the Inner Detector [1], of radius $\sim$ 1m, built for precision tracking and vertexing. The inner detector consists of the following:

- the Pixel Detector (silicon pixel detectors)
- the Semiconductor Tracker (silicon strip detectors) [2]
- the Transition Radiation Tracker (TRT) (straw detectors)

There are in total 2112 modules on the SCT barrel structure. There are 12 modules in a line along the length of the barrel, and 32, 40, 48 and 56 modules round the circumference of the four barrels (moving outwards) respectively. To reduce systematic error on particle tracking, it is important to know the position of the modules very accurately. The target alignment accuracy of the modules is of the order 12 microns [1].

The precise determination of the module positions is the crucial element to assure the maximum performance on the ID tracking. ATLAS aims to achieve the high precision in coordinate determination by performing alignment using information from the reconstructed tracks. The alignment algorithms are based on minimizing the hit residuals; the distances between hits on the modules and the fitted track positions at each module. Two examples of track-based alignment algorithms currently commissioned in ATLAS are Global χ^2 and Robust Alignment [3, 4].

The track-based alignment algorithms require a sufficiently precise knowledge of the initial module positions to converge on accurate and precise final values. This is provided by surveys during the construction of the modules, as well as during initial commissioning while the detectors are put in place. In this note, we examine the measurements from photogrammetry survey performed during assembly of the SCT barrels and compare the survey data with alignment parameters determined from cosmic ray data. During ATLAS operation, any changes in the shape of the SCT detector structure are monitored by the hardware-based FSI alignment system [5], so that corrections can be applied in the tracking algorithms. The FSI corrections are calculated using interpolation procedures similar to those described in this note, which were developed initially for analysis of the photogrammetry survey.

2.2 The Surveys

Three separate photogrammetry surveys were carried out on the SCT barrels to check the engineering alignment of the structure:

Survey 1 [6]: This is the most detailed survey of the three, and was carried out on 14.11.2005 before the SCT was installed into ATLAS. It recorded the relative position of the eight radial interlinks that support the four cylinders at either end of the barrel, as well as the FSI targets and pixel supports. Four external reference targets were also surveyed. Survey 1 had an x-y precision of 20 μm.

Survey 2 [7]: A second survey recorded a change of the external reference targets, with a precision of 100 μm, before the SCT was inserted into the TRT.

Survey 3 [8]: A third survey was recorded just after the SCT had been inserted into the TRT, with an estimated precision of 150 μm, before and after an adjustment to the concentricity of the detectors.

This investigation involves the data from the first survey [6] only. A photogrammetric system measured the position of reflective targets that were mounted in precisely machined hole locations at the extremities of the SCT structure. The positions of the targets were determined to 20 μm in the x and y direction, and 40 μm in the z direction at the σ level. The locations were chosen to help constrain the SCT cylinder to cylinder placement, the FSI end flange component placement and the location of Pixel jig. Raw data is detailed in the appendix.

Data points 2106, 2108, 4106 and 4108 are very far removed from the others. This is due to the mechanical photogrammetry target being a relatively long way from the SCT barrel compared to the other targets; not due to any mistake in the survey. However, for simplicity, these data points have been removed for the remainder of the analysis.

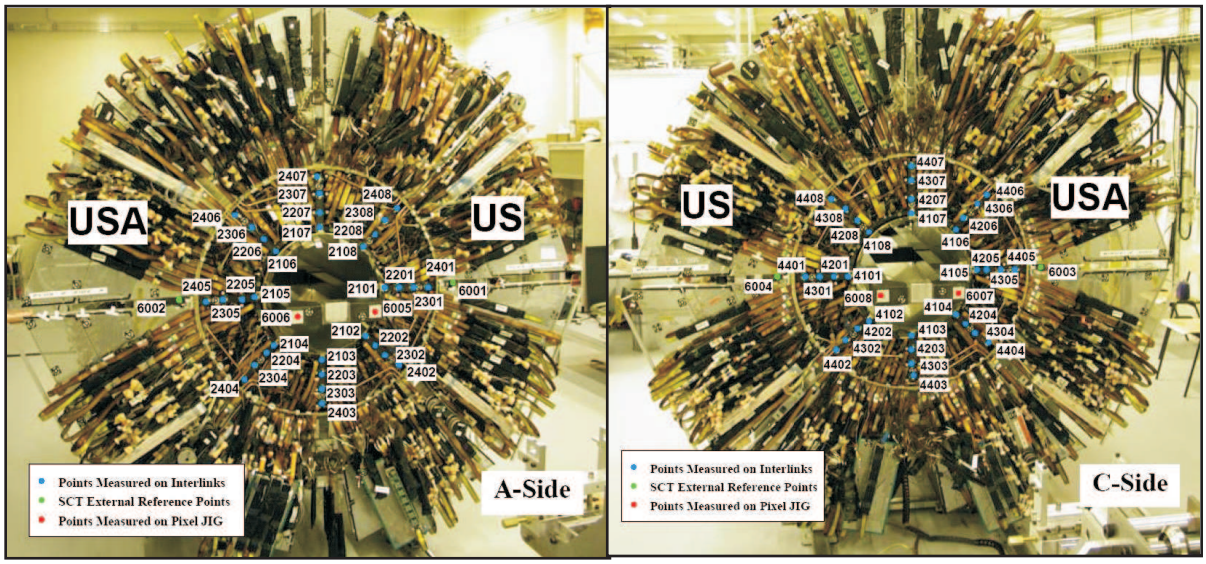

Figure 1: Details of the photogrammetry survey [6]

3 SCT Barrel deformation

3.1 Preliminary analysis

Data from the first photogrammetry survey of the SCT Barrel were initially analysed by the CERN survey group, who released the processed data as an EDMS note [6]. The primary aim of this analysis was to check the build precision of the SCT, particularly the concentricity of the barrel layers. Circle fits and mean planes were calculated for the eight photogrammetry targets on each end-face (A,C) and layer (1-4), giving the results in Table 1.

	Centre of circle			Diff to Circle			Diff to Plane	
Name	X (m)	Y (m)	Z (m)	rad (m)	Min (mm)	Max (mm)	Min (mm)	Max (mm)
A1	0.00002	0.00000	0.78289	0.29002	-0.08	0.05	-0.13	0.19
A2	-0.00003	0.00001	0.78293	0.34096	-0.05	0.05	-0.04	0.08
A3	0.00001	0.00004	0.78290	0.41347	-0.04	0.06	-0.07	0.07
A4	0.00000	-0.00001	0.78291	0.48446	-0.05	0.05	-0.02	0.04
C1	0.00001	0.00000	-0.78300	0.28998	-0.12	0.12	-0.17	0.18
C2	0.00000	-0.00002	-0.78291	0.34099	-0.10	0.07	-0.08	0.05
C3	0.00000	0.00000	-0.78288	0.41349	-0.11	0.10	-0.09	0.07
C4	0.00001	0.00002	-0.78288	0.48443	-0.13	0.08	-0.13	0.06

Table 1: Summary results of circle and mean plane fits to survey data [6]

Importantly, the four SCT cylinders were found to be concentric and their axes aligned to well within the engineering tolerances. In fact, the centres of all the circle fits to each barrel face and layer are identical to within a few tens of micrometers in the transverse x-y plane. However, the radial differences between the measured points and the circle fits are typically much larger, up to around ± 100 μm. The radial deviations are statistically significant compared the measurement resolution per point of ± 20 μm. The possibility that there was a correlated spatial pattern to these radial deviations stimulated the study below.

3.2 Radial deformation

The four carbon-fibre cylinders of the SCT barrel are fastened together using eight radial interlink bars at each end-face of the barrel. The photogrammetry targets were located at the intersection of the barrel layers and the interlinks. The following correlations were revealed by plotting the radial deviations of the measured targets from the circle fits to each barrel layer, as a function of physical layout, as shown in Figure 2:

- The radial deviations of all four points on any one interlink are typically well correlated.
- The eight points on any barrel layer are shifted in a correlated pattern such that each layer forms an ellipse.
- The size and direction of the major axes of the ellipses formed by each barrel layer are similar between layers on the same face.
- The major axes of the ellipse on each face has an angular offset with respect to the vertical (y-axis), and is of opposite sign for each face of the barrel.

The elliptical correlations are clarified by plotting the average radial shift of each interlink as a function of the azimuthal position of the interlink, as in Figure 3. The interlink positions for each face form an approximately sinusoidal pattern, with differing amplitude and phase for each face. The amplitude of the average deviations for Face C, at around 100 μm, is approximately twice that for Face A. The phase difference is estimated to be 35 degrees. The observed correlations suggest a radial deformation with progressive twist along length of the barrel structure. A likely cause of this deformation is proposed in section 3.4.

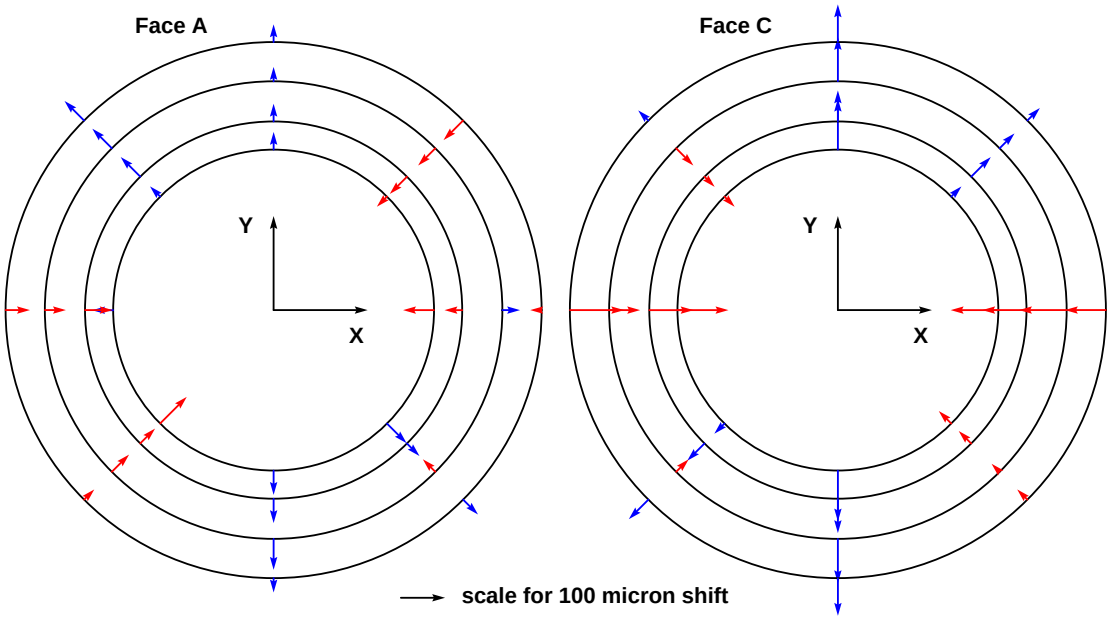

Figure 2: *Radial deviation between the measured photogrammetry targets and the circle fits to each barrel layer. The shifts are drawn to scale, exaggerated for clarity by the* 100 μm *factor shown.*

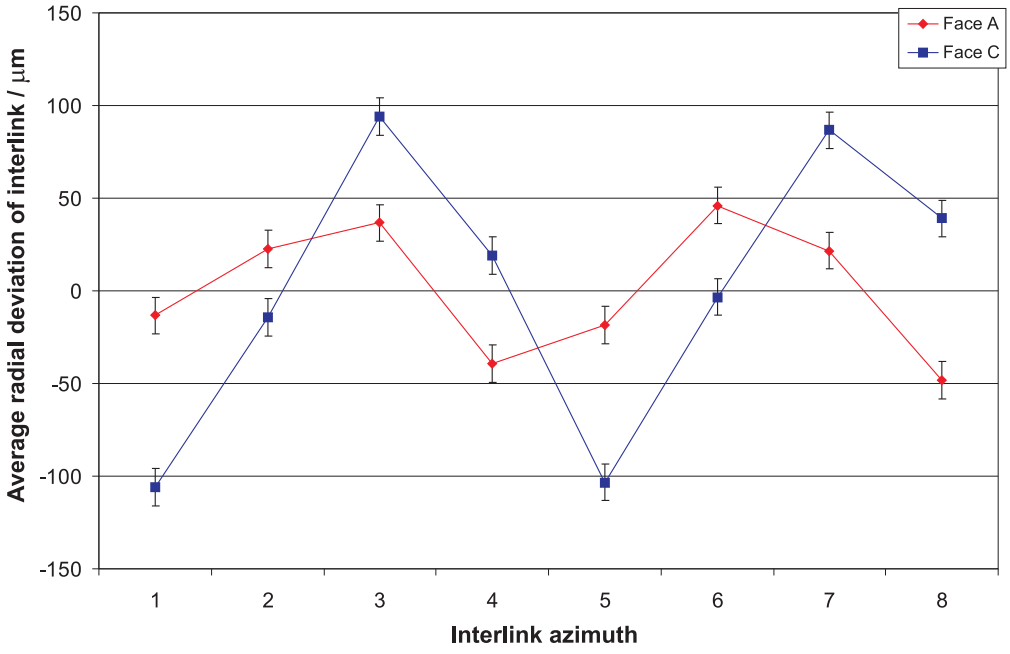

Figure 3: *Surveyed average radial deviation of each SCT interlink as a function of azimuth.*

3.2.1 Ellipse fitting

A further investigation of the deformation was performed by fitting ellipses to each barrel layer and face in the x-y plane, using the general quadratic form of an ellipse,

$$ax^2 + by^2 + cxy + dx + ey + f = 0. \quad (1)$$

The measurement precision of ± 20 μm was assumed for the input errors to the ellipse fit algorithm. The stability of convergence of the algorithm was checked by performing pseudo-fits on randomly generated data sets, in which the target positions were smeared by ± 20 μm errors about the measured x and y points of the interlinks. The stability of the fit was then compared to extracted fit errors, for the x and y coordinates. The Monte Carlo agreed with the errors on the fit parameters. In all the fits, $\chi^2/dof < 1$, which indicates that the input errors (± 20 μm) might be an overestimate.

Figure 4 shows the results of the ellipse fits, for face A. The normally scaled fitted ellipses have an eccentricity very close to zero, so the radial deviations has been plotted with an exaggerated scale for clarity. Separate circle fits are overlaid (in black) to guide the eye for the possible deformation.

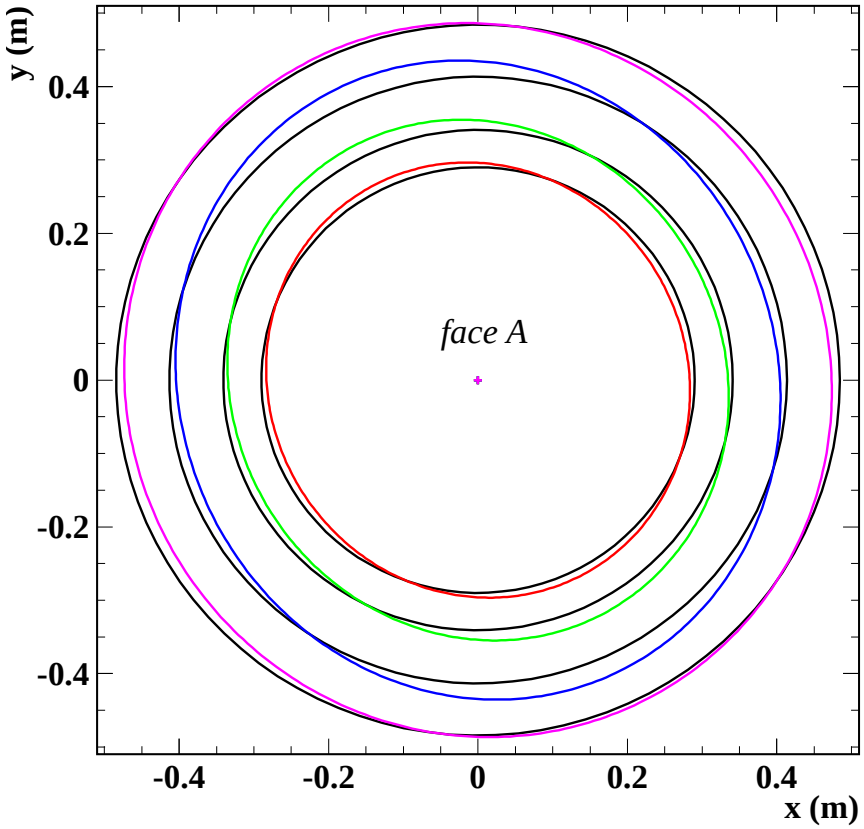

Figure 4: *Elliptical fits to the SCT barrel layers. The radial deviations are to an exaggerated scale for clarity.*

The results of the ellipse fits are presented in Table 2. We note that the results for the smallest barrel (layer 1) should be disregarded because the fit did not omit the two target points which were by construction offset from

the nominal circle of the SCT barrel layer, as in section 2.2. With the exception of this first layer, the centres of the fitted ellipses match very well the centres of the circle fits that were performed by the CERN survey group, as in Table 1.

	Centre of ellipse		Ellipse axes:			Tilt
Name	X (m)	Y (m)	semi-minor (m)	semi-major (m)	D(maj-min) (μm)	(deg)
A1	-0.000004	-	0.28567	0.28580	128.6	125.3
A2	-0.000026	0.000011	0.34091	0.34101	102.0	113.3
A3	-0.000011	0.000039	0.41343	0.41351	72.2	118.2
A4	-0.000005	-0.000010	0.48442	0.48449	76.8	123.5
C1	0.000019	-	0.28558	0.28582	239.6	85.8
C2	-0.000005	-0.000018	0.34090	0.34108	179.2	80.8
C3	0.000001	0.000004	0.41340	0.41358	187.7	85.1
C4	0.000009	0.000016	0.48434	0.48453	192.6	85.2

Table 2: Results of ellipse fits to measured survey points by barrel layer (1-4) and face (A/C).

The ellipses formed by each barrel layer are found to be remarkably similar within each barrel face. The differences between the semi-major and semi-minor axis, thus the total maximum to minimum radial deviation for each barrel layer is typically around 100 μm for face A and 200 μm for face C. This agrees the amplitudes of the sinusoidal variation of the average interlink radial deviations that were plotted in Figure 3. The average tilt angle of the major ellipse for 120^o and 84^o for faces A and C respectively, giving a phase difference between the faces of 36^o, also in agreement with the previous plot.

3.3 Angular distortion

Ideally, the eight data points for each face and barrel should be at $\phi = n\pi/4$ where n = 0,7,6,5,4,3,2,1 which is the order the points are tabulated in appendix A. The deviation in $\bar{R}\phi$, $\bar{R}\Delta\phi$, from this ideal positioning was calculated in μm, where $\bar{R}$ is calculated as the radius of a circle fit for each of the eight data points in that particular layer and face. These calculations are summarised in Table 3 and comparison of the $\bar{R}\Delta\phi$ values to those obtained from track based alignment methods is given in section 7. Averaging over the four layers on each face gives and RPhi difference between the two faces of 28 μm.

Name	Radius from circle fit/m	Average $\Delta\phi$/mrad	Average $(\bar{R}\Delta\phi)/\mu$m	Average $(\bar{R}\Delta\phi)/\mu$m (wrt layer 0)
A1	0.29002	0.0863	19.6	0.0
A2	0.34096	0.1350	46.0	26.4
A3	0.41347	0.0258	10.7	-8.9
A4	0.48446	-0.0215	-11.3	-8.2
C1	0.28998	0.0466	4.2	0.0
C2	0.34099	-0.0321	-10.9	6.7
C3	0.41349	-0.0215	-8.9	4.7
C4	0.48444	-0.0753	-36.5	-40.7

Table 3: Average barrel rotation in the Rϕ direction

3.4 Interpretation of the deformation

The observed correlations suggest two possible interpretations:

- either, that there was a consistent, systematic error in the manufacture of all barrel layers, for example a misalignment during the machining of holes for the interlinks in the barrels flanges. However, this is considered unlikely to generate the different groups of ellipses parameters at either end of the barrel, as found above.
- or, more likely, that there was a global deformation of the structure when the survey was taken. This hypothesis is supported by the predictions of a Finite Element Analysis model used to design the SCT Barrel, that pre dates the survey. The FEA model predicted that a global deformation of the observed type could occur for certain structural support conditions, as described in below.

The SCT barrel is nominally mounted on four points which are at the ends of the two horizontal lines passing through the centres of the two barrel end-faces. The four points are designed to lie in the same horizontal plane. However, this is difficult to achieve exactly in practice, so typically one corner point will be slightly below the other three points. The barrel is not perfectly rigid so it deforms to rest on all four points. The shape it makes when it does this, in the one we believe the survey revealed: namely elliptical radial deformations at either barrel end, with a progressive twist from one end to the other. In the worst case, if the fourth points is very out of plane, the structure will deform maximally and will lose contact with the fourth point. This 3-point mount scenario was previously modelled using Finite Element Analysis [9], as shown in Figure 5. The maximum deflection of 369 μm in this case is larger than the observed $\pm$100 μm in our study, implying that the barrel was indeed supported by all four points during the survey, but that the supports points did not lie perfectly in a plane.

It is important to note that the measured "twist" of 36^o from end to end is only in the shape of the radial deformations and certainly does not indicate a similar magnitude twist in the Rϕ positions of the barrel modules. Despite the large radial deformation which has a twisted shape, there was found to be a relatively small (on average 28 μm from end to end) Rϕ twist of the modules along the cylinder surface.

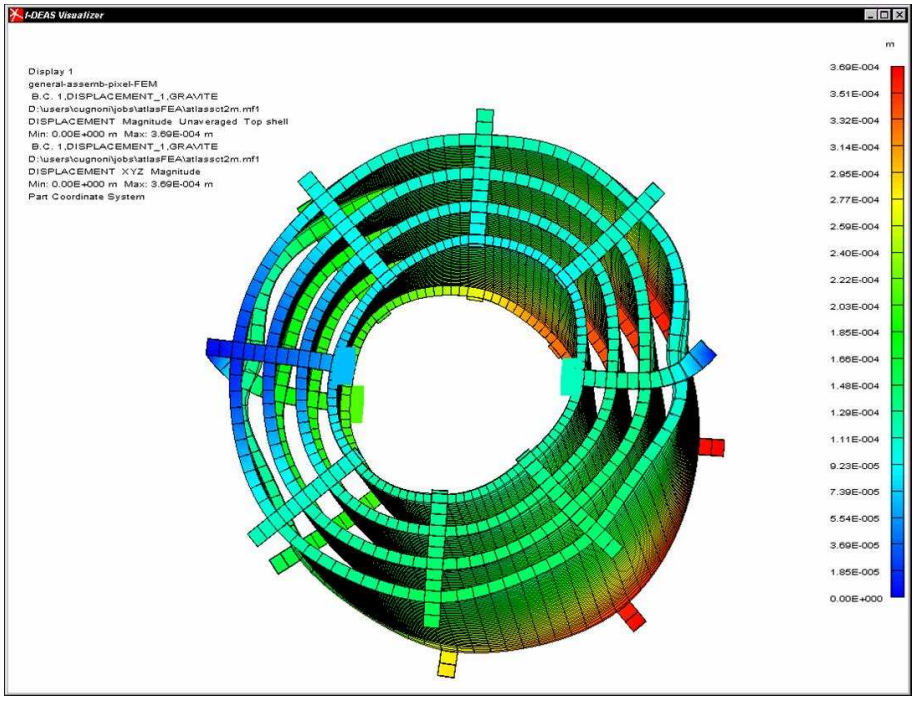

Figure 5: *Deformation of SCT barrel assembly with temporary 3 point supports. Maximal dflection (free end of the interlink): 369 microns.[9]*

4 Interpolating to module positions

An interpolation to predicted module positions is necessary in order to compare the photogrammetry results to track based alignment methods. The procedure was as follows:

4.1 General Procedure

The photogrammetry data was interpolated to simulate the positions of the modules on the SCT barrels using the following procedure:

Step one: Data point at angle ϕ on face A joined by a straight line to the corresponding point on face B. Lines drawn between the two points at each angle (eight lines for each barrel, thirty two for four barrels)

Step two: Each line separated into twelve equally spaced points, corresponding to the twelve rings of modules on the SCT barrel. Each point is now labelled by ring number (from -6 $\rightarrow$ -1 and 1 $\rightarrow$ 6) and layer number (from 0 $\rightarrow$ 3, corresponding to the SCT barrels.

Step three: The eight points[1] at each ring and layer number are then fitted as an ellipse. The reported 20 μm error was fed into the TMinuit fitting programme (for all data points [x' y']). The above assumes that each fitted ellipse is centered on the point (0,0). This is a valid assumption, as it may be seen from the circle fits in [6] that the offsets of the fitted circles are very small with respect to the magnitude of the data points.

The χ^2 values show that an ellipse fit is significantly better than a circle fit for all rings and layers, thus confirming the hypothesis that the barrel deformation is of an elliptical nature. The rest of the report thus assumes that the deformation is of an elliptical nature. With only eight data points in each fit, consideration of higher eigenmodes of deformation were not needed.

Step four: Increment round the circumference of the fitted ellipse (starting at ϕ=0) in equal increments of arc length to obtain the module positions. The incrementation must be done using numerical methods (100,000 increments of arc length are used).

4.2 Radial distance between data points and ellipse fits

It is interesting to obtain a measure of the radial distortion between the nominal positions and data points, and the surface of the fitted ellipse. Figure 6 shows the radial deviation between the raw data points interpolated data points from the fitted ellipse. The radial deviation from the ellipse fit is of the order 50 microns and it has been seen that this does not degrade as one moves down the barrel in the z direction.

4.2.1 Properties of the fitted ellipses

The mean eccentricity was 0.24 with an RMS value of 0.006. This gives us an idea of the scale of deformation involved. As a back of the envelope calculation, we imagine that the length of the major axis, B, of the fitted ellipse is of the order 1m. In this case, the length of the minor axis will be given by A. Taking the RMS value of the eccentricity we see that this length is approximately 999.4mm. Thus the maximum distortion (difference in length between the major and minor axes) we expect in an ellipse is approximately 0.6mm.

The angles of the fitted ellipses are shown in figure 7. We see that the angle of rotation for the ellipse fit is pointing in the opposite direction in face A than in face C. The fitted ellipses that are between face A and C have a gradually rotating angle, as one would expect.

[1] six points in layer 0 due to the anomalous data points

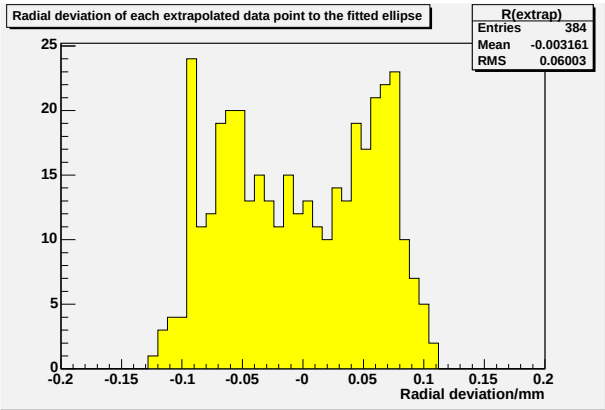

Figure 6: Radial Deviation between the data and the fitted ellipse

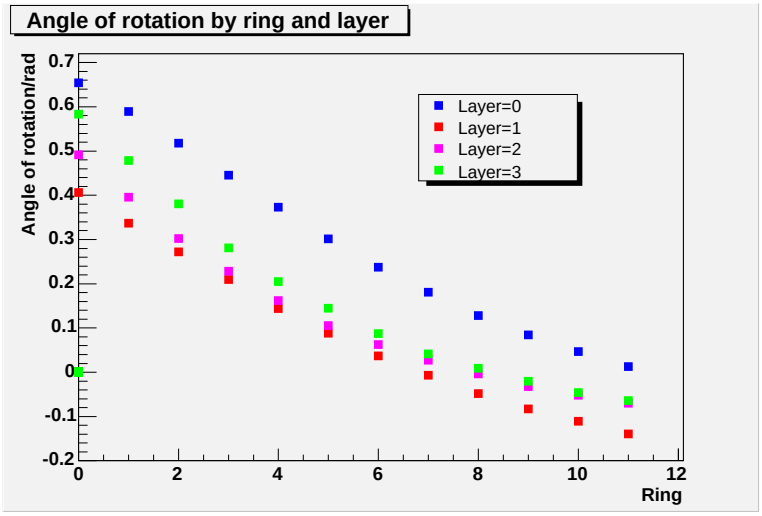

Figure 7: Angle of rotation of each fitted ellipse

5 Generation of nominal module positions

To mirror the procedure that will be followed in the FSI interpolation, it is necessary to compare the simulated module positions with the nominal. Simulated nominal module positions must first be generated for this. Based on the assumption that the SCT nominal structure is cylindrical the circle fits made by the CERN team [6] were used to increment, in equal amounts of θ starting at θ=0, around faces A and C by the number of modules on each circle in each layer of the SCT. The module coordinates on each face were interpolated in 12 equal increments along the length of the barrel in the z direction, as before. This procedure yielded a set of 2112 coordinates to be used as the nominal module coordinates.

6 Overlap of neighbouring modules

The following two chapters investigate the behaviour of $\Delta\Delta\phi$, a quantity which is defined on the diagram in figure 8. $\Delta\phi$ is the angular spacing between neighbouring modules on the same ring and layer. $\Delta\Delta\phi$ is a measure of the spacing of the simulated module coordinates on the ellipse circumference with respect to the nominal 'circle' spacing, and is a quantity to which track based alignment methods (namely the robust alignment and global χ^2 methods) may be sensitive.

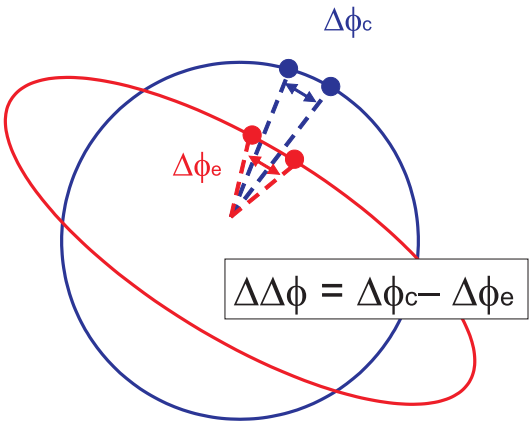

Figure 8: Definition of $\Delta\Delta\phi$

Figure 9 shows the distribution of the difference, $\Delta\Delta\phi$, between $\Delta\phi_c$ of two neighbouring modules in the circle fit, and $\Delta\phi_e$ of the corresponding neighbouring modules in the ellipse fit, as is defined in figure 8. The magnitude of this quantity yields a measure of whether the distortions that are seen in the photogrammetry data are of sufficient magnitude to be seen in a track based alignment.

We see in figure 9[2] that the RMS value of the distribution is $\simeq 20$ μrad. We recall that the barrel radius is of order 0.5m, and thus this would correspond to a value R$\phi \simeq 10\mu$m. Given that track based methods are sensitive to distortions of order 10 μm and above, this places the data right at the boundary of whether it may be seen or not by such methods. Further investigation might be carried out.

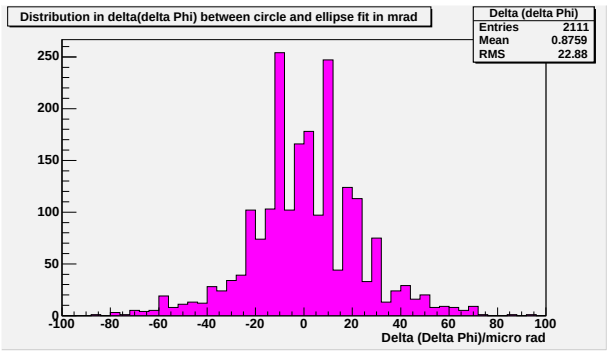

Figure 9: Distribution of $\Delta\Delta\phi$ between simulated ellipse module and nominal circle module.

[2]The discontinuous nature of the distribution is due to a combination of the quadrant symmetry of the ellipse and the finite number of increments used during the incrementation procedure.

6.1 Variation of $\overline{\Delta\Delta\phi}$ with z

The distributions of $\Delta\Delta\phi$ were investigated as a function of z (ie for each ring).

To compare with the track based alignment from the cosmic data the data was plotted only from the range in ϕ used. A definite overall bias in the value of $\Delta\phi$ was seen in both of these ranges. This is what is expected for this type of elliptical deformation. An overall bias will be seen, and will be positive or negative dependent on whether we are close to the major or minor axis of the ellipse. The fact that in this range the bias is positive tells us that we are close to the minor axis, as it means the spacing of the modules on the ellipse is greater than the spacing of the modules in the nominal. The error on the mean value in these plots is smaller than in the overall plot. This is also expected, as much larger smearing would be present over a full range in ϕ.

One would expect, if the same plot was made in the previous range plus π radians, that the overall bias would be negative, as the ellipse modules would be closer together than the nominal. These positives and negatives will cancel out to give an overall $\Delta\Delta\phi$ of zero. It is possible to carry out further investigation of this effect, for example to predict from the data the eccentricity of the ellipse upon which the modules lie. However we stop at this point as the effect is too small to be seen by track based analysis of the cosmics data.

6.2 Variation of $\overline{\Delta\Delta\phi}$ with ϕ

The behaviour of $\Delta\Delta\phi$ were investigated as a function of ϕ. Firstly, the deviation of all modules from the nominal in ϕ, multiplied by the mean radius of the barrel upon which the module sits, were plotted as a function of ϕ. The values were binned into twelve equal bins of ϕ starting at $\phi = 0$ (so that each bin of phi has width $\frac{2\pi}{12}$, and the phi value may be recovered from the bin value using the formula Angle = $\frac{BinNumber\times\pi}{6}$).

A sinusoidal deviation with ϕ of $\overline{\Delta\Delta\phi}$ was seen. This may be modelled with four free parameters, which are related to the properties of the sin wave as follows; A(amplitude), B(inverse wavelength), C(phase) and D(offset in the y direction).

$$\overline{\Delta\Delta\phi} = A\sin(B\phi + C) + D, \tag{2}$$

This sinusoidal behaviour is a direct property of how the modules are spaced on the circumference of an ellipse, compared to that of a circle, as a function of ϕ. If the modules are placed at constant increments of ϕ (which they are), their spacing round the circumference of an ellipse will vary sinusoidally, whereas the same quantity around the circumference of a circle will be constant. Thus $\Delta\Delta\phi$ will also behave as a sinusoid. This sinusoidal behaviour is an effect which may be seen by the cosmic data and analysis, and so we investigate how the parameters of these sinusoids behave as we vary R and z.

6.2.1 Behaviour with z: ordering by ring

To see the variation of the sinusoids with z, the plots in Figure 10 were repeated but split up into four sections of z; rings [-6 → -4], [-3 → -1], [1 → 3] and [4 → 6]. The resulting sinusoids were fitted using formula 2 and the values of A, B, C and the χ^2 values of the fit displayed in Table 4. We see that the sinusoidal effect increases in both amplitude and phase (and a very slight increase in offset) along the barrel in z. The increase in phase is a result of the rotation of the ellipse fit from the xy axes with z, as shown in Figure 7. The increase in amplitude is due to a (very small) increase in eccentricity.

The plots have been manipulated into a form such that it is possible to compare with results obtained from track based analysis of the cosmic data. However, as explained earlier, this is only available over certain ranges, and thus dotted lines have been drawn on the plots to show where these cuts would be placed.

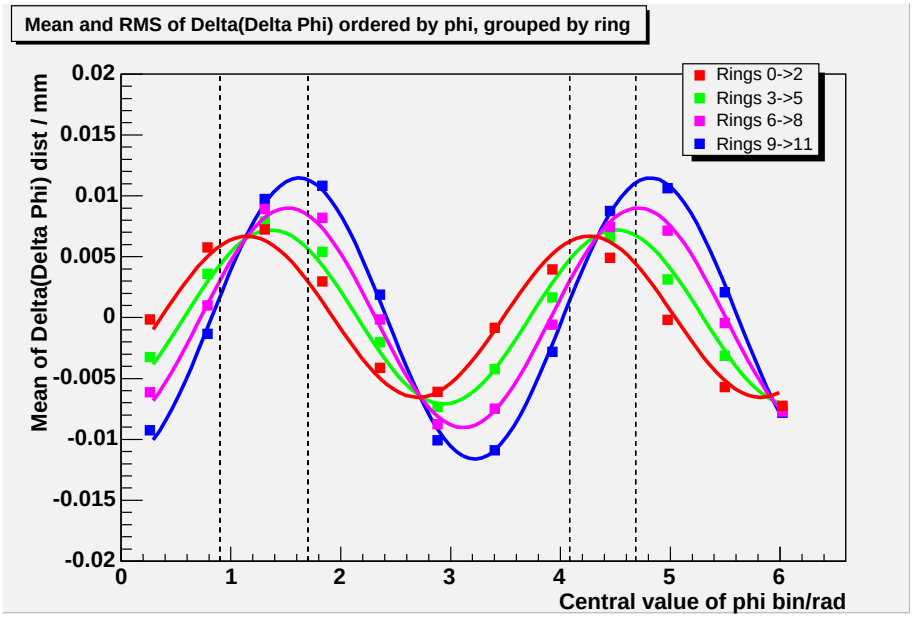

Figure 10: Statistics of distribution of $\Delta\Delta\phi$ with ϕ arranged in twelve sections of ϕ. The dotted lines show the regions of ϕ sensitive to cosmics data.

Ring Section	A (amplitude)	B (wavelength)	C (phase)	D(Y offset)	χ^2
-6 → -4	0.006 (±0.0003)	2.02 (±0.022)	-0.76 (±0.08)	-0.00002 (±0.0002)	10.26
-3 → -1	0.007 (±0.0002)	2.00 (±0.020)	-1.16 (±0.071)	-0.000002 (±0.0002)	8.12
1 → 3	0.009 (±0.0002)	1.97 (±0.017)	-1.43 (±0.061)	-0.0002 (±0.0002)	4.72
4 → 6	0.011 (±0.0003)	1.96 (±0.02)	-1.61 (±0.056)	-0.0001 (±0.0002)	3.21

Table 4: Parameters of the sin fit of $\Delta\Delta\phi$ with ϕ obtained for four sections of z.

6.2.2 Radial behaviour: ordering by layer

Figure 11 shows the resultant distribution split layer by layer, again with the cosmic data cuts shown as a dotted line on the graph. Given that there is one wavelength in a $0 \rightarrow \pi$ range, a moment's thought will convince the reader that the 'B' parameter, the 'inverse wavelength' from equation 2 should be equal to 2. Two fits were done on the data; one with four free parameters as before, and one where the B parameter was fixed to 2.

The resultant fit parameters and χ^2 values (normalised correctly according to the number of free parameters in the fit) are shown in Table 5. We see in the table that whether B is fixed or is allowed to be fitted directly does not substantially affect the fit.

The fits tell us that there is a decrease in amplitude of the sinusoid as we move radially outwards in layer.

Layer	NBins	A	B	C	D	chisq
0	30	0.016 (±0.0002)	1.87 (±0.011)	5.40 (±0.047)	-0.0009 (±0.0002)	11.67
0	30	0.015 (±0.0002)	2 (fixed)	5.00 (±0.025)	-0.0003 (±0.0002)	34.75
1	38	0.009 (±0.0002)	2.13 (±0.012)	4.28 (±0.036)	0.0004 (±0.0001)	19.20
1	38	0.009 (±0.0002)	2 (fixed)	4.64 (±0.018)	0.00002 (±0.0001)	41.99
2	46	0.008 (±0.0002)	1.97 (±0.012)	4.75 (±0.037)	-0.00007 (±0.0001)	52.40
2	46	0.008 (±0.0002)	2 (fixed)	4.68 (±0.016)	0.0001 (±0.0001)	52.37
3	54	0.006 (±0.0001)	1.94 (±0.01)	5.01 (±0.034)	-0.0001 (±0.00009)	9.51
3	54	0.006 (±0.0001)	2 (fixed)	4.87 (±0.020)	0.00009 (±0.00008)	12.98

Table 5: Parameters of the sinusoidal fit of $\Delta\Delta\phi$ with ϕ in four layers

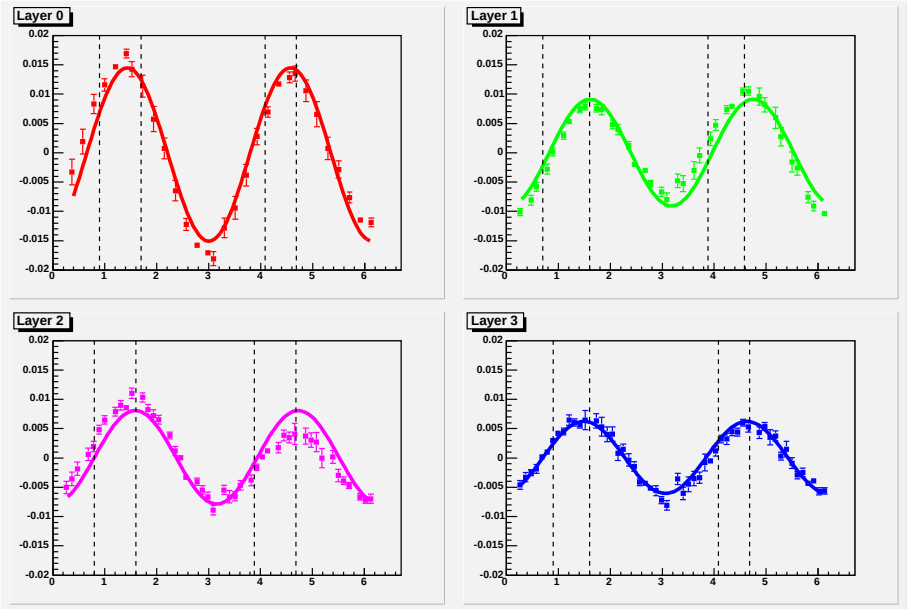

Figure 11: Distribution of $\Delta\Delta\phi$, arranged by ϕ and grouped by layer. B parameter is fixed at 2.

7 Comparison with track based alignment analysis on cosmics data

A health warning must be emphasised with the following analysis; as is explained in Section 2, the cosmics data were taken after the barrel had been moved to be positioned in the TRT, following the initial photogrammetry survey. The fact that the barrel has moved between the two sets of data taking must be kept in consideration.

7.1 Comparison of quantity $\bar{R}\Delta\phi$

The mean of the two average values of $\bar{R}\Delta\phi$ (as defined in Table 3) for layer 0 was taken as a reference point. The same value for each layer was calculated, and the reference point subtracted to give four values[3] per each layer (black curve in Figure 12. This gives an idea as to the size of the rotation of the entire barrel, with respect to the other barrels and can be used to compare photogrammetry data with track-based alignment methods.
The other two curves in the figure are results from robust alignment and global χ^2 methods. The two track based methods appear to agree each other but have little or no correlation with the photogrammetry data. However, the track values were calculated using old cosmics alignment constants which could be the source of the discrepancy.

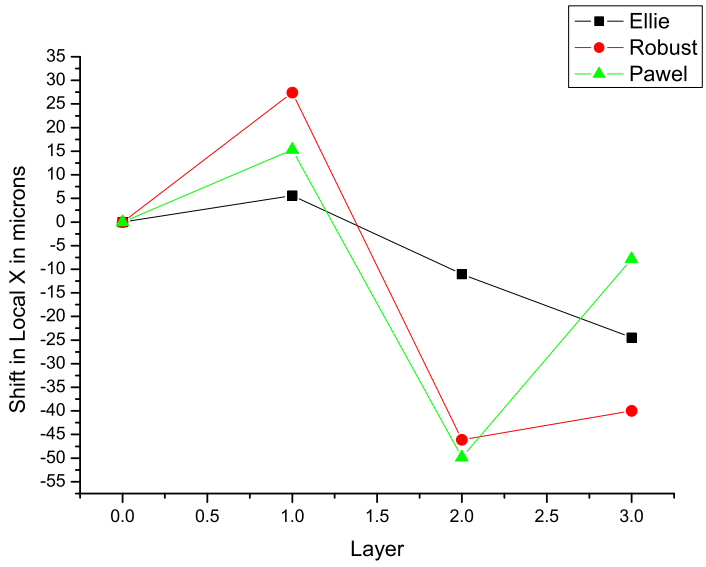

Figure 12: Average $\bar{R}\Delta\phi$ found for each layer, with comparison to robust alignment and global χ^2 methods.

[3] 0, 5.6355, -11.0200, -35.8182 μm for layers 0,1,2,3 respectively

7.2 Comparison of fits in $\Delta\Delta\phi$ with ϕ

The data obtained using track based methods (with the phase and y offset also fixed) are shown in Figure 13. To facilitate direct comparison with the cosmic data, the fit was reattempted only with data within the range dictated by the cosmics allowed in the fit. The resultant fit parameters are shown in Table 6. Due to the severe constraints this imposes on the amount of data allowed in the fit, it was necessary to fix the B parameter to 2 (which, as we saw before, does not substantially alter the quality of the fit in a full data range) and also the D parameter to 0 (which, again as seen before, is always 0 within errors in a full data range).

Due to the restriction on the range of data, the χ^2 values will always be very bad. To see if there is any real evidence in the restricted range of data to a sin wave, another linear fit was also performed so that the χ^2 values may be compared:

$$y = Ex + F. \tag{3}$$

The E and F values of the fit, along with the χ^2 values, are also shown in Table 6. We see that in all layers apart from 2, data is described better with a sinusoidal curve with respect to a linear regession. This suggests that even in the limited acceptance to the cosmic ray data, it should be possible to see some sort of sin pattern. However, we notice no correlation (either by eye or studying the parameters of the fit) between the track fits and the photogrammetry fits. This leads to one of two possible conclusions; either that the data range is too limited to make a meaningful fit to the data or that the discrepancy in fits is due to the fact that the barrel moved between the survey and cosmic data taking runs.

Layer	Method	A	B	C	D	E	F	χ^2 sin	χ^2 lin
0	PG	-0.015 ($\pm$0.0005)	2	1.76 ($\pm$0.06)	0	-0.0010($\pm$0.0002)	0.016($\pm$0.0005)	2.24	23.11
0	Robust	-0.029 ($\pm$0.0072)	2	-6.25 ($\pm$0.25)	0	N/A	N/A	1.46	N/A
0	χ^2	-0.030 ($\pm$0.0121)	2	-1.83 ($\pm$0.25)	0	N/A	N/A	13.47	N/A
1	PG	-0.009 ($\pm$0.0004)	2	1.53 ($\pm$0.04)	0	-0.0010($\pm$0.0002)	0.016($\pm$0.0005)	35.05	67.60
1	Robust	-0.039 ($\pm$0.0028)	2	-0.61 ($\pm$0.15)	0	N/A	N/A	2.22	N/A
1	χ^2	-0.046 ($\pm$0.0120)	2	0.91 ($\pm$0.12)	0	N/A	N/A	3.34	N/A
2	PG	-0.009 ($\pm$0.0003)	2	1.45 ($\pm$0.03)	0	-0.0020($\pm$0.0001)	0.010($\pm$0.0003)	45.11	42.85
2	Robust	-0.042 ($\pm$0.0032)	2	-1.13 ($\pm$0.13)	0	N/A	N/A	3.70	N/A
2	χ^2	-0.110 ($\pm$0.0060)	2	-1.52 ($\pm$0.06)	0	N/A	N/A	11.8	N/A
3	PG	-0.005 ($\pm$0.0003)	2	1.86 ($\pm$0.10)	0	-0.0001($\pm$0.0001)	0.005($\pm$0.0004)	3.24	8.35
3	Robust	-0.011 ($\pm$0.0041)	2	-4.72 ($\pm$0.36)	0	N/A	N/A	3.01	N/A
3	χ^2	-0.064 ($\pm$0.0093)	2	-1.12 ($\pm$0.28)	0	N/A	N/A	2.76	N/A

Table 6: Fits of $\Delta\Delta\phi$ with ϕ in four layers only using data in cosmics range. The parameter B is fixed at 2 and D fixed at 0. 'PG' refers to the photogrammetry data.

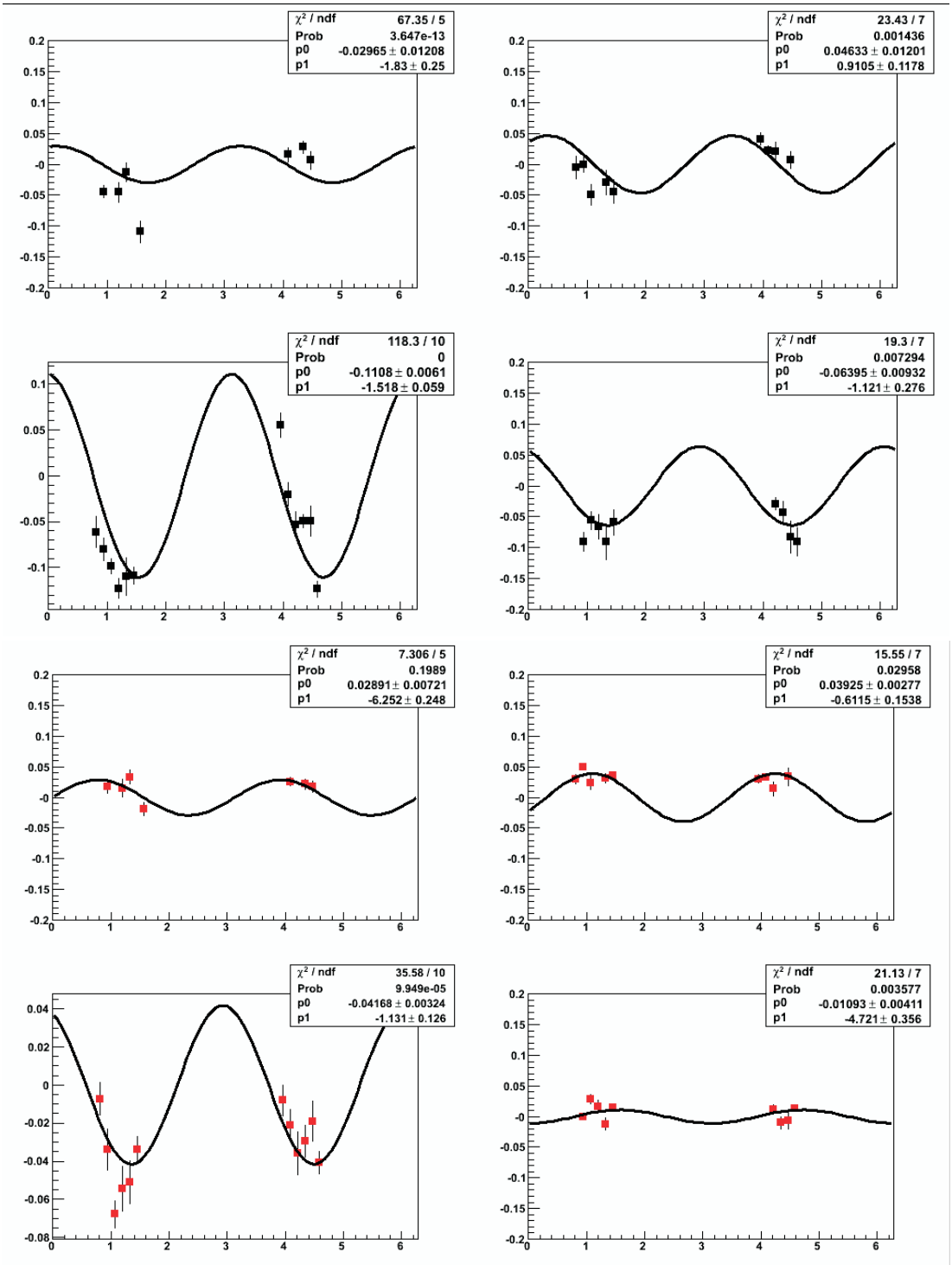

Figure 13: Distribution of $\Delta\Delta\phi$ from track based methods, arranged by ϕ and grouped by layer. The fit is done with a phase fixed at 2 and a y offset fixed at 0. The upper four plots are the results from the global χ^2 and the lower four from the robust alignment methods.

8 Summary and Conclusions

The photogrammetry survey has identified that although the SCT barrel layers are very concentric, there are genuine radial deformations of the SCT structure. Elliptical radial deformations with an amplitude of around ± 100 μm are observed at the ends of the barrel, with a progressive twist of 36^o in the ellipse axis from one end to the other. A corresponding average Rϕ twist around the cylinder surface of 28 μm was found between barrel ends. The global shape of this deformation matches predictions from a Finite Element Analysis model in which the four mounting points of the SCT do not lie in a perfect plane. It was seen that this type of distortion will show a characteristic sinusoidal pattern in $\Delta\Delta\phi$, where the phase and amplitude are related to the eccentricity and rotation of the ellipse in a predictable manner. The cosmic data were insufficient to see the same effect due to the small ranges in ϕ covered. The SCT support conditions also changed after the survey and before the cosmic data were taken. However, the plots produced here may be made during ATLAS operations, to identify the type of barrel distortion observed here.

References

[1] ATLAS Inner Detector TDR

[2] Atlas SemiConductor Tracker Barrel

[3] F. Heinemann: Robust Track Based Alignment of the ATLAS Silicon Detector and Assessing Parton Distribution Uncertainties in Drell-Yan Processes, University of Oxford, 2007

[4] P. Bruckman, A. Hicheur, S. Haywood: Globalχ^2 approach to the alignment of the ATLAS silicon tracking detectors, 2004, ATL-INDET-PUB-2005-002

[5] S.M. Gibson *et al.*, Opt. Lasers Eng. 43 815, 2005; P.A. Coe *et al.*, Meas. Sci. Technol. 15 2175, 2004

[6] https://edms.cern.ch/document/681215; EDMS ATL-IS-UR-0004 (ID 681215)

[7] https://edms.cern.ch/document/705191; EDMS ATL-IS-UR-0004 (ID 705191)

[8] https://edms.cern.ch/document/708009; EDMS ATL-IS-UR-0004 (ID 708009)

[9] J. Cugnoni, E. Perrin, "ATLAS SCT Assembly Finite Element Analysis", Universite de Geneve / EPFL, Lausanne, 18 June 2001.

A Raw Data from the survey

Name	X(m)	Y(m)	Z(m)
2101	0.28998	-0.00006	0.78285
2102	0.20504	-0.20519	0.78318
2103	0.00002	-0.29005	0.78286
2104	-0.20509	-0.20493	0.78283
2105	-0.29003	-0.00024	0.78284
2106	-0.19267	0.19276	0.78285
2107	0.00007	0.29004	0.78287
2108	0.19267	0.19261	0.78284
2201	0.34091	-0.00010	0.78289
2202	0.24107	-0.24112	0.78291
2203	0.00004	-0.34099	0.78290
2204	-0.24115	-0.24101	0.78301
2205	-0.34094	0.00000	0.78290
2206	-0.24106	0.24124	0.78290
2207	-0.00001	0.34100	0.78295
2208	0.24110	0.24102	0.78298
2301	0.41350	-0.00003	0.78278
2302	0.29239	-0.29229	0.78291
2303	0.00003	-0.41349	0.78279
2304	-0.29235	-0.29227	0.78297
2305	-0.41343	0.00006	0.78287
2306	-0.29234	0.29249	0.78300
2307	-0.00001	0.41352	0.78292
2308	0.29232	0.29240	0.78294
2401	0.48445	0.00001	0.78287
2402	0.34259	-0.34258	0.78288
2403	0.00003	-0.48447	0.78289
2404	-0.34254	-0.34258	0.78295
2405	-0.48442	0.00004	0.78292
2406	-0.34258	0.34261	0.78292
2407	-0.00002	0.48446	0.78290
2408	0.34248	0.34256	0.78294
4101	0.28988	-0.00005	-0.78293
4102	0.20498	-0.20510	-0.78292
4103	0.00002	-0.29010	-0.78289
4104	-0.20500	-0.20509	-0.78316
4105	-0.28984	-0.00006	-0.78288
4106	-0.19260	0.19272	-0.78287
4107	0.00002	0.29009	-0.78316
4108	0.19271	0.19270	-0.78280
4201	0.34088	0.00001	-0.78292
4202	0.24102	-0.24120	-0.78297
4203	0.00000	-0.34108	-0.78291
4204	-0.24117	-0.24114	-0.78295
4205	-0.34089	-0.00012	-0.78290
4206	-0.24112	0.24109	-0.78292
4207	0.00000	0.34103	-0.78294
4208	0.24108	0.24120	-0.78280
4301	0.41338	0.00004	-0.78288
4302	0.29239	-0.29236	-0.78295
4303	-0.00002	-0.41359	-0.78291
4304	-0.29238	-0.29236	-0.78302
4305	-0.41343	-0.00004	-0.78281
4306	-0.29233	0.29238	-0.78287
4307	0.00001	0.41359	-0.78283
4308	0.29237	0.29244	-0.78274
4401	0.48435	0.00007	-0.78291
4402	0.34252	-0.34255	-0.78295
4403	0.00005	-0.48450	-0.78291
4404	-0.34255	-0.34258	-0.78283
4405	-0.48430	-0.00004	-0.78287
4406	-0.34256	0.34256	-0.78292
4407	-0.00004	0.48453	-0.78293
4408	0.34251	0.34264	-0.78275

Table 7: Raw data obtained from photogrammetry survey [6]